



## Full Text View

[Volume 32, Issue 5 \(May 2002\)](#)

### Journal of Physical Oceanography

 Article: pp. 1452–1459 | [Abstract](#) | [PDF \(295K\)](#)

# Intrusions in Double-Diffusively Stable Arctic Waters: Evidence for Differential Mixing?

**William J. Merryfield**

*Institute of Ocean Sciences, Sidney, British Columbia, Canada*

(Manuscript received July 10, 2001, in final form September 28, 2001)

DOI: 10.1175/1520-0485(2002)032<1452:IIDDSA>2.0.CO;2

### ABSTRACT

Intrusions like those observed in double-diffusively stable regions of the Arctic Ocean can grow from uniform ambient temperature and salinity gradients if diapycnal mixing of these two components differs. Assuming this to be the driving mechanism, the observed 40–60 m intrusion heights constrain the turbulent diffusivity for heat to be less than about  $0.01 \text{ cm}^2 \text{ s}^{-1}$  and the salt-to-heat turbulent diffusivity ratio to be greater than about 0.6 if the diffusivities are constant. Observations indicate that the intrusions slope across isopycnals in a sense that is consistent with such a scenario, although the along-intrusion density ratio is greater than that predicted by linear theory for the fastest-growing intrusions. Numerical solutions for growing intrusions resemble observed temperature and salinity profiles.

### 1. Introduction

Warm, salty water of Atlantic origin circulates cyclonically around the perimeters of Arctic Ocean basins, giving rise to pronounced lateral contrasts in temperature  $T$  and salinity  $S$  ([Rudels et al. 1994](#)). According to recent observations, this water interleaves with colder, fresher central basin waters, transporting  $T$  and  $S$  across the large-scale gradients ([Anderson et al. 1994](#); [Carmack et al. 1997](#); [Rudels et al. 1999](#)). The associated intrusions can be coherent across entire basins ([Carmack et al. 1999](#)).

The warm, salty core of the Atlantic influence resides at around 300-m depth. Conditions above the core favor diffusive convection, which transports  $T$  more effectively than  $S$ , whereas conditions beneath it favor salt fingering, which transports  $S$  more effectively than  $T$  ([Schmitt 1994](#)). These unequal vertical transports of  $S$  and  $T$  are known to promote intrusion growth when lateral gradients are also present ([Stern 1967](#); [Toole and Georgi 1981](#); [Walsh and Ruddick 1995](#)).

#### Table of Contents:

- [Introduction](#)
- [Theory versus observation](#)
- [Numerical simulation](#)
- [Conclusions](#)
- [REFERENCES](#)
- [TABLES](#)
- [FIGURES](#)

#### Options:

- [Create Reference](#)
- [Email this Article](#)
- [Add to MyArchive](#)
- [Search AMS Glossary](#)

#### Search CrossRef for:

- [Articles Citing This Article](#)

#### Search Google Scholar for:

- [William J. Merryfield](#)

What is perhaps surprising is that intrusive features are seen also at depths between about 700 and 1100 m or more, where  $T$  decreases and  $S$  increases downward, so that double diffusion is not active. [This is termed the Upper Polar Deep Water (UPDW) by [Rudels et al. \(1994\)](#).] [Figure 1](#) shows an example of this phenomenon in data from the *Oden 91* expedition ([Anderson et al. 1994](#)). Such intrusions, bracketed here by the dotted lines, have been found at numerous widely spaced locations in the Amundsen, Makarov, and Nansen Basins ([Anderson et al. 1994](#); [Rudels et al. 1994](#); [Carmack et al. 1999](#)).

Under these bistable conditions, vertical mixing is believed to result mainly from occasional shear instabilities of internal gravity waves ([Garrett 1979](#); [Gargett 1989](#)). In ocean circulation models, such mixing typically is represented as diffusion with equal coefficients  $K_T$  and  $K_S$  for  $T$  and  $S$ . However, the presence of intrusions in the UPDW could be an indication that  $K_T \neq K_S$ , as discussed below.

Interest in whether  $K_S/K_T$  can depart from unity under double-diffusively stable conditions stems from a need for accurate mixing parameterizations for ocean circulation models, and from observed model sensitivities to this parameter ([Gargett and Holloway 1992](#); [Gargett and Ferron 1996](#); [Zhang et al. 1998](#); [Merryfield et al. 1999](#)). The possibility of unequal  $K_T$  and  $K_S$  is supported by laboratory ([Turner 1968](#); [Altman and Gargett 1990](#)) and numerical experiments ([Merryfield et al. 1998](#)), which indicate that  $K_T$  can exceed  $K_S$  because of the greater molecular diffusivity for  $T$  ( $\kappa_T \approx 1.4 \times 10^{-3} \text{ cm}^2 \text{ s}^{-1}$ ) than for  $S$  ( $\kappa_S \approx 1.5 \times 10^{-5} \text{ cm}^2 \text{ s}^{-1}$ ).

This paper demonstrates that intrusions indeed arise under bistable conditions when mixing of  $T$  and  $S$  is unequal, and attempts to infer mixing properties from observed properties of the intrusions, assuming they are diffusively driven. A linear stability analysis is first employed in [section 2](#) to constrain values for  $K_T$  and  $K_S$ , which reproduce the observed 40–60 m intrusion heights. The plausibility of inferred  $K_T$  and  $K_S$ , as well as intrusion growth rate, is then assessed. Observed intrusions are shown to rise across isopycnals as they get warmer and saltier, in agreement with theory, although the observed along-intrusion density ratio is larger than predicted. A nonlinear computation of intrusion growth and equilibration is compared with observed  $T$  and  $S$  profiles in [section 3](#), and conclusions are presented in [section 4](#).

## 2. Theory versus observation

### a. Stability calculations

The stability theory for intrusions in a bistable environment resembles that for intrusions driven by salt fingering, as developed by [Stern \(1967\)](#), [Toole and Georgi \(1981\)](#), and [Walsh and Ruddick \(1995\)](#). Consider an infinite medium at rest, having uniform vertical temperature and salinity gradients  $\bar{T}_z$  and  $\bar{S}_z$ , and horizontal gradients  $\bar{T}_x$  and  $\bar{S}_x$ . The equation of state is assumed to be linear, so that

$$\rho = \rho_0[1 - \alpha(T - T_0) + \beta(S - S_0)], \quad (1)$$

where  $\rho$  is density;  $\alpha$  and  $\beta$  are coefficients of thermal expansion and haline contraction; and  $\rho_0$ ,  $T_0$ , and  $S_0$  are constant reference values. The horizontal gradients are assumed to be density compensating, so that  $\alpha\bar{T}_x = \beta\bar{S}_x$ . Baroclinic effects (e.g., [May and Kelley 1997](#)) and viscous–diffusive instability ([McIntyre 1970](#)) are not considered. Following [Walsh and Ruddick \(1995\)](#), the linearized Boussinesq equations describing perturbations ( $\psi$ ,  $T'$ ,  $S'$ ) are written

$$\nabla^2 \psi_t = g(\alpha T'_x - \beta S'_x) + (A\psi_{xz})_{xz} + (A\psi_{zz})_{zz}, \quad (2)$$

$$T'_t - \bar{T}_x \psi_z + \bar{T}_z \psi_x = (K_T T'_z)_z, \quad (3)$$

$$S'_t - \bar{S}_x \psi_z + \bar{S}_z \psi_x = (K_S S'_z)_z, \quad (4)$$

where  $g$  is gravitational acceleration,  $A$  is effective viscosity, and streamfunction  $\psi$  is related to  $x$ - and  $z$ -velocity components  $u$  and  $w$  by  $u = -\psi_z$  and  $w = \psi_x$ . [Rotation is neglected in (2) because it does not affect the wavelength, growth rate, or cross-frontal slope of the fastest-growing mode ([McDougall 1985](#); [Kerr and Holyer 1986](#)).] [Equations \(2\)–\(4\)](#) differ from [Eq. \(8\)](#) of [Walsh and Ruddick \(1995\)](#) in that  $K_T$  and  $K_S$  are specified independently instead of being linked by a double-diffusive flux ratio. In addition,  $\bar{S}_z$  is presumed here to be negative, rather than positive.

To account for possible dependence of  $K_T$  and  $K_S$  upon Brunt–Väisälä frequency  $N = (-g\rho_z/\rho)^{1/2}$ , functional forms

$$K_T = K_T^0 \left( \frac{N}{N_0} \right)^\mu, \quad K_S = K_S^0 \left( \frac{N}{N_0} \right)^\mu, \quad \mu = 0, -1 \quad (5)$$

are considered, where  $N_0$  applies to the undisturbed state (Table 1). The choice  $\mu = 0$  implies constant  $K_T$  and  $K_S$ , whereas  $\mu = -1$  has been suggested by Gargett (1984) and Gargett and Holloway (1984). Coefficient  $A$  is specified in terms of a turbulent Prandtl number  $\text{Pr} \equiv (A - \nu)/(K_T - \kappa_T)$ .

Substituting  $(\psi, T', S') = (\hat{\psi}, \hat{T}, \hat{S})e^{i(kx+mz)+rt}$  into (2)–(5) leads to a linear eigenvalue problem for  $r$ , with characteristic polynomial

$$\begin{aligned} & \tilde{r}^3 + \tilde{r}^2 [1 + \sigma + \tau + (R_\rho - \tau')\Delta] \tilde{m}^2 \tilde{K}_T \\ & + \tilde{r} \left\{ [\sigma\tau + (\sigma + \tau - \tau'\Delta)(1 + R_\rho\Delta) + \tau'\Delta(R_\rho\Delta - \sigma)] \right. \\ & \quad \left. \times \tilde{m}^4 \tilde{K}_T^2 + \frac{s^2}{1 + s^2} \right\} \\ & + \frac{s^2}{1 + s^2} \left[ \frac{(\tau - 1)(\Gamma_S + sR_\rho)}{R_\rho - 1} + s \right] \tilde{m}^2 \tilde{K}_T \\ & + [(1 + R_\rho\Delta)(\tau - \tau'\Delta) + \tau'R_\rho\Delta^2] \sigma \tilde{m}^6 \tilde{K}_T^3 = 0, \quad (6) \end{aligned}$$


where  $\tilde{r} = rN_0^{-1}$ ,  $\tilde{m} = m(K_*/N)^{1/2}$ , and  $\tilde{K}_T = K_T/K_*$  in which  $K_* = 1.0 \text{ cm}^2 \text{ s}^{-1}$ ,  $\sigma = A/K_T$ ,  $\tau = K_S/K_T$ ,  $\tau' = K'_S/K'_T$ , and  $\Delta = K'_T/K_T(R_\rho - 1)$  in which  $K'_T = dK_T/dN$  and  $K'_S = dK_S/dN$ ;  $\Gamma_S = \bar{S}_x/\bar{S}_z$  is isohaline slope; and  $s = k/m$  is the intrusion slope. In the following, coefficients  $\alpha$  and  $\beta$  and gradients  $\bar{T}_x$ ,  $\bar{S}_x$ ,  $\bar{T}_z$ , and  $\bar{S}_z$  in (6) are assigned representative observed values (Table 1), and mixing parameters  $K_T^0$ ,  $K_S^0$ , and  $\text{Pr}$  are varied. In all cases horizontal and vertical wave numbers  $k$  and  $m$  are assigned which maximize growth rate  $r$ .

The above analysis yields positive growth rates when  $\tau < 1$ , as may occur for weak turbulent mixing. The growing intrusions rise or sink across isopycnals more shallowly than the isohalines (Fig. 2). Rising intrusions in this “wedge” are cooler and fresher than their surroundings. Because the cool anomaly that retards their rise diffuses more rapidly than the fresh anomaly that drives it, the intrusions become positively buoyant and grow. The nature of such intrusions is discussed in detail by Hebert (1999), who considered cases in which diffusive  $T$  and  $S$  fluxes are linked by a constant ratio and in which  $K_T$  and  $K_S$  are assigned constant values with no dependence on local stratification. (The latter case is equivalent to the present analysis with  $\mu = 0$ .)

### b. Intrusion wavelengths and growth rates


Figure 3 shows predicted intrusion heights  $\lambda = 2\pi/m$  in meters as a function of  $K_T$  and  $K_S/K_T$  for  $\text{Pr} = 2$ , with  $\mu = 0$  (Fig. 3a) and  $\mu = -1$  (Fig. 3b). Values lying within the observed range 40–60 m appear in bold face. The curves approximate the dependence of  $K_S/K_T$  on  $K_T$ , which was found for individual mixing events in numerical experiments of Merryfield et al. (1998). If such events are intermittent in space and time, effective  $K_T$  is reduced, whereas  $K_S/K_T$  is unaffected. The curves thus indicate approximate lower limits to  $K_S/K_T$  for a given  $K_T$ , according to the Merryfield et al. (1998) results.

With  $\mu = 0$  (Fig. 3a), the bold-faced values coinciding with observed  $\lambda$  intersect the curve near  $K_T = 0.01 \text{ cm}^2 \text{ s}^{-1}$  and

$K_S/K_T = 0.6$ , which represent an upper limit to  $K_T$  and a lower limit to  $K_S/K_T$  if the foregoing assumptions are correct. With  $\mu = -1$  (Fig. 3b ) , the bold-faced values intersect the curve near  $K_T = 0.03 \text{ cm}^2 \text{ s}^{-1}$  and  $K_S/K_T = 0.7$ . In both panels, admitted values for  $K_T$  and  $K_S/K_T$  are indicated schematically by the hatched regions.

The implied values  $K_T \approx 0.01 \text{ cm}^2 \text{ s}^{-1}$  for  $\mu = 0$  and  $K_T \approx 0.03 \text{ cm}^2 \text{ s}^{-1}$  for  $\mu = -1$  are somewhat lower than  $K_T \approx 0.1$  inferred for the midlatitude pycnocline (e.g., [Ledwell et al. 1993](#)). However, the Arctic Ocean is relatively quiescent with respect to internal waves, and such low values may be plausible ([D'Asaro and Morison 1992](#)).


Growth rates within the hatched regions peak at about  $(2 \text{ yr})^{-1}$  near their intersections with the dashed curves, and decrease with decreasing  $K_T$  and increasing  $K_S/K_T$ . For intrusions to grow appreciably, the residence time of the UPDW must exceed a few growth periods. Although this residence time is not well known, the few existing deep Arctic current observations indicate speeds of less than  $1 \text{ cm s}^{-1}$  away from major topographic features ([Aagaard 1981](#)). Dividing an approximate basin circumference of 3000 km by  $1 \text{ cm s}^{-1}$  suggests residence times exceeding 10 years, which is compatible with growth periods of a few years or less.

The above results are not especially sensitive to  $Pr$ , which is not well known, but which probably lies between 1 and its molecular value of about 7. For example,  $\lambda = 55 \text{ m}$  for  $Pr = 5$  versus  $46 \text{ m}$  for  $Pr = 2$  when  $K_T = 0.01 \text{ cm}^2 \text{ s}^{-1}$ ,  $K_S/K_T = 0.6$ , and  $\mu = 0$  (Table 2 ) .

### c. Along-intrusion density ratio

As a further test of whether intrusion properties are consistent with driving by differential turbulent mixing with  $K_T > K_S$ , the along-intrusion density ratio  $R_I \equiv (\alpha \partial T / \partial l) / (\beta \partial S / \partial l)$ , where  $l$  is along-intrusion distance, is examined. For intrusions having slope  $s \ll 1$ ,

$$R_I \approx \frac{\Gamma_s + sR_\rho}{\Gamma_s + s}. \quad (7)$$


Assigning parameter values as in [section 2b](#) yields the predicted values for  $R_I$  shown in [Fig. 4](#) .

The allowed range of  $R_I$  for growing intrusions can be deduced in much the same manner as in [Ruddick \(1992\)](#), who considered intrusions driven by double diffusion in a Mediterranean salt lens. Setting the dimensionless growth rate  $\tilde{\Gamma}$  to zero in dispersion relation (6) and solving for minimum and maximum allowed  $s \ll 1$  at marginal stability yields

$$0 < s < \frac{\Gamma_s(1 - \tau)}{1 - \tau R_\rho}, \quad (8)$$

which translates to

$$1 < R_I < \tau^{-1}. \quad (9)$$

Numerical determinations of  $R_I$  for fastest-growing intrusions are shown in [Fig. 4](#) . For  $K_T$  and  $K_S/K_T$  consistent with results of [Merryfield et al. \(1998\)](#) and yielding intrusion heights within the observed range (hatched regions),  $1 \approx R_I \approx 1.1$ .






By comparison, the theory of [Toole and Georgi \(1981\)](#), which links vertical fluxes according to a fixed flux ratio

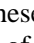
$$\frac{K_T \alpha \partial T / \partial z}{K_S \beta \partial S / \partial z} \equiv \gamma, \quad (10)$$

as is found for double diffusion, yields an allowed range

$$1 < R_I < \gamma, \quad (11)$$

when  $\gamma > 1$  (cf. [Ruddick 1992](#)).

In an attempt to infer  $R_I$  from observations, six stations from the *Oden 91* expedition were considered ([Table 3](#) ). Each is located in the interior of the Amundsen Basin well away from the Lomonosov and Gakkel ridges ([Anderson et al. 1994](#)), and typically they are spaced 100 to 200 km apart. [Figure 5](#)  shows data from the UPDW plotted on the  $T$ - $S$  plane, with positive and negative salinity extrema of individual intrusions labeled by filled and open circles. Contours of  $\sigma_1 = \rho_1 - 1000$  are indicated, where  $\rho_1$  is potential density referenced to 1000-db pressure. It is evident that intrusions tend to rise across isopycnals as they become warmer and saltier, consistent with driving by  $K_T > K_S$  as illustrated in [Fig. 2](#) . Linear fits to positive and negative extrema for each intrusion are shown in [Fig. 6](#) . These fits imply values for  $R_I$  ranging from 1.05 to 2.03, all consistent with driving by  $K_T > K_S$ . (These values could contain an alongfront contribution to  $R_I$  that is not accounted for in the stability analysis; this is assumed not to be the case.) Average  $R_I$  based on positive extrema is 1.66, and on negative extrema is 1.53; the grand average  $R_I = 1.60$ . This value is consistent with [\(9\)](#) if  $\tau \approx 0.62$ , but is significantly larger than the range  $1 \approx R_I \approx 1.1$  suggested by [Fig. 4](#) .

Applying a similar fitting procedure to  $T$  and  $S$  as functions of pressure indicates that the intrusions tend generally to rise across isobars as they become warmer and saltier ([Fig. 7](#) ), although the considerable scatter in these relations as well as the unevenness of horizontal  $T$  and  $S$  gradients between stations precludes a confident determination of slope. However, the fact that the intrusions rise across isobars and isopycnals as they become warmer and saltier indicates that their slope lies outside the wedge of baroclinic instability, and suggests that baroclinicity does not contribute to the driving mechanism (e.g., [May and Kelley 1997](#)).


### 3. Numerical simulation

To simulate the growth and equilibration of intrusions in the UPDW, the nonlinear Boussinesq equations were solved in a tilted reference frame aligned with the intrusions. As shown by [Walsh and Ruddick \(1998\)](#), this enables the problem to be cast in terms of a single spatial coordinate. The one-dimensional equations derived by [Merryfield \(2000\)](#) are

$$Z_t = -g \sin\theta(\alpha T' - \beta S')_{\zeta} + \cos^2\theta(AZ)_{\zeta\zeta}, \quad (12)$$

$$T'_t = -U(\bar{T}_x \cos\theta + \bar{T}_z \sin\theta) + \cos^2\theta(K_T T'_{\zeta})_{\zeta}, \quad (13)$$

$$S'_t = -U(\bar{S}_x \cos\theta + \bar{S}_z \sin\theta) + \cos^2\theta(K_S S'_{\zeta})_{\zeta}, \quad (14)$$

where  $\zeta$  is distance perpendicular to the intrusions,  $U = -\psi_{\zeta}$  is along-intrusion velocity,  $Z = \psi_{\zeta\zeta}$ , and  $\theta = -\tan^{-1}s$ . As intrusions grow, gradients may cease to be double-diffusively stable. In such instances,  $K_T$ ,  $K_S$ , and  $A$  are specified as in [Table 4](#) , with  $K_{\text{conv}} = 5 \text{ cm}^2 \text{ s}^{-1}$ ,

$$K_S^f = 0.17(1 - \tau_f R_{\rho}) / (R_{\rho} - \gamma_f) \text{ cm}^2 \text{ s}^{-1} \quad (15)$$

with  $\tau_f \equiv \kappa_S / \kappa_T = 0.01$ ,  $\gamma_f = 0.6$  ([Merryfield and Grinder 2000](#), unpublished manuscript) and

$$K_T^d = 3.2 \times 10^{-3} \kappa_T [0.25 \times 10^9 R_{\rho}^{-1.1}]^{1/3} \\ \times \exp(4.8 R_{\rho}^{0.72}) \text{ cm}^2 \text{ s}^{-1} \quad (16)$$

with

$$\gamma_d = \frac{R_{\rho}^{-1} + 1.4(R_{\rho}^{-1} - 1)^{3/2}}{1 + 14(R_{\rho}^{-1} - 1)^{3/2}}, \quad (17)$$

([Kelley 1990](#)). Background  $K_T$  and  $K_S$  are constant ( $\mu = 0$ ), and double-diffusive processes are assumed not to contribute to  $A$ , as laboratory experiments suggest ([Ruddick et al. 1989](#)). [Equations \(12\)–\(17\)](#) were solved pseudospectrally on a 64-point grid spanning one intrusion, as described in [Merryfield \(2000\)](#). Initial conditions consisted of random, density compensating perturbations to  $T$  and  $S$  having rms amplitudes of about 0.1% of the top-to-bottom property contrasts and a

red spectrum. (Initial perturbations having blue spectra yielded identical equilibrated states.) [Figures 8a,b](#) show the representative case  $K_T^0 = 0.01 \text{ cm}^2 \text{ s}^{-1}$ ,  $K_S^0/K_T^0 = 0.65$ ,  $\text{Pr} = 2$ , and  $\mu = 0$ . The stack of six intrusions shown represents a periodic extension of the single-intrusion numerical solution; offsets in  $T$ ,  $S$ , and depth have been introduced to facilitate comparison with data from *Oden* 91 station 31 in Amundsen Basin, shown in [Figs. 8c,d](#). Initially, the intrusions have grown with an  $e$ -folding time of 2.0 yr, as predicted by linear theory. At an intermediate stage of growth, intrusion amplitudes are similar to those observed (solid curves), whereas three years later the intrusions are nearing equilibration at larger amplitudes still (dotted curves).

#### 4. Conclusions

The presence of intrusions in the UPDW does not prove that double-diffusively stable turbulence mixes  $T$  and  $S$  unequally. Additional influences not considered here may include baroclinicity ([May and Kelley 1997, 2001](#)), viscous–diffusive instability ([McIntyre 1970](#)), and propagation from a remote origin ([Schadlow et al. 1992](#)). However, the present results show that intrusions resembling those observed can be achieved diffusively for plausible values of  $K_T$  and  $K_S/K_T$ , although the discrepancy between observed and predicted along-intrusion density ratios needs to be explained.

#### Acknowledgments

The *Oden* 91 CTD dataset was kindly provided by Peter Jones. Ann Gargett and Greg Holloway provided helpful suggestions for improving the manuscript, as did Brian May, Barry Ruddick, and an anonymous reviewer. This work was supported by the Office of Naval Research (N00014-99-1-0050).

---

#### REFERENCES

- Aagaard K., 1981: On the deep circulation of the Arctic Ocean. *Deep-Sea Res.*, **28A**, 251–268. [Find this article online](#)
- Altman D. B., and A. E. Gargett, 1990: Differential property transport due to incomplete mixing in a stratified fluid. *Stratified Flows*, E. J. List and G. H. Jirka, Eds., American Society of Civil Engineers, 454–460.
- Anderson L. G., Coauthors, 1994: Water masses and circulation in the Eurasian Basin: Results from the *Oden* 91 expedition. *J. Geophys. Res.*, **99**, 3273–3283. [Find this article online](#)
- Carmack E. C., Coauthors, 1997: Changes in temperature and tracer distributions within the Arctic Ocean: Results from the 1994 Arctic Ocean section. *Deep-Sea Res.*, **44**, 1487–1502. [Find this article online](#)
- Carmack E. C., K. Aagaard, J. H. Swift, R. G. Perkin, F. A. McLaughlin, R. W. Macdonald, and E. P. Jones, 1999: Thermohaline transitions. *Physical Processes in Lakes and Oceans, IUTAM Proceedings*, J. Imberger, Ed., Amer. Geophys. Union, 179–186.
- D'Asaro E. A., and J. H. Morison, 1992: Internal waves and mixing in the Arctic Ocean. *Deep-Sea Res.*, **39**, 459–S484, S. [Find this article online](#)
- Gargett A. E., 1984: Vertical eddy diffusivity in the ocean interior. *J. Mar. Res.*, **42**, 359–393. [Find this article online](#)
- Gargett A. E., 1989: Ocean turbulence. *Annu. Rev. Fluid Mech.*, **21**, 419–451. [Find this article online](#)
- Gargett A. E., and G. Holloway, 1984: Dissipation and diffusion by internal wave breaking. *J. Mar. Res.*, **42**, 15–27. [Find this article online](#)
- Gargett A. E., 1992: Sensitivity of the GFDL ocean model to different diffusivities for heat and salt. *J. Phys. Oceanogr.*, **22**, 1158–1177. [Find this article online](#)
- Gargett A. E., and B. Ferron, 1996: The effects of differential vertical diffusion of  $T$  and  $S$  in a box model of thermohaline circulation. *J. Mar. Res.*, **54**, 827–866. [Find this article online](#)
- Garrett C., 1979: Mixing in the ocean interior. *Dyn. Atmos. Oceans*, **3**, 239–265. [Find this article online](#)
- Hebert D., 1999: Intrusions: What drives them? *J. Phys. Oceanogr.*, **29**, 1382–1391. [Find this article online](#)
- Kelley D. E., 1990: Fluxes through diffusive staircases: A new formulation. *J. Geophys. Res.*, **95**, 3365–3371. [Find this article online](#)
- Kerr O. S., and J. Y. Holyer, 1986: The effect of rotation on double-diffusive interleaving. *J. Fluid Mech.*, **162**, 23–33. [Find this article online](#)

- Ledwell J. R., A. J. Watson, and C. S. Law, 1993: Evidence for slow mixing across the pycnocline from an open-ocean tracer release experiment. *Nature*, **364**, 701–703. [Find this article online](#)
- May B. D., and D. E. Kelley, 1997: Effect of baroclinicity on double-diffusive interleaving. *J. Phys. Oceanogr.*, **27**, 1997–2008. [Find this article online](#)
- May B. D., 2001: Growth and steady state stages of thermohaline intrusions in the Arctic Ocean. *J. Geophys. Res.*, **106**, 16783–16794. [Find this article online](#)
- McDougall T. J., 1985: Double-diffusive interleaving. Part I: Linear stability analysis. *J. Phys. Oceanogr.*, **15**, 1532–1541. [Find this article online](#)
- McIntyre M. E., 1970: Diffusive destabilization of the baroclinic circular vortex. *Geophys. Fluid Dyn.*, **1**, 19–57. [Find this article online](#)
- Merryfield W. J., 2000: Origin of thermohaline staircases. *J. Phys. Oceanogr.*, **30**, 1046–1068. [Find this article online](#)
- Merryfield W. J., G. Holloway, and A. E. Gargett, 1998: Differential vertical transport of heat and salt by weak stratified turbulence. *Geophys. Res. Lett.*, **25**, 2773–2776. [Find this article online](#)
- Merryfield W. J., 1999: A global ocean model with double-diffusive mixing. *J. Phys. Oceanogr.*, **29**, 1124–1142. [Find this article online](#)
- Ruddick B. R., 1992: Intrusive mixing in a Mediterranean salt lens—Intrusion slopes and dynamical mechanisms. *J. Phys. Oceanogr.*, **22**, 1274–1285. [Find this article online](#)
- Ruddick B. R., R. W. Griffiths, and G. Symonds, 1989: Frictional stress across a sheared double-diffusive interface. *J. Geophys. Res.*, **94**, 18161–18173. [Find this article online](#)
- Rudels B., E. P. Jones, L. G. Anderson, and G. Kattner, 1994: On the intermediate depth waters of the Arctic Ocean. *The Role of the Polar Oceans in Shaping Global Climate*, O. M. Johannessen, R. D. Muench, and J. E. Overlans, Eds., Amer. Geophys. Union, 33–46.
- Rudels B., G. Björk, R. D. Muench, and U. Schauer, 1999: Double-diffusive layering in the Eurasian Basin of the Arctic Ocean. *J. Mar. Syst.*, **21**, 3–27. [Find this article online](#)
- Schadow S. G., E. Thomas, and J. R. Kosleff, 1992: The dynamics of intrusions into a thermohaline stratification. *J. Fluid Mech.*, **236**, 127–165. [Find this article online](#)
- Schmitt R. W., 1994: Double diffusion in oceanography. *Annu. Rev. Fluid Mech.*, **26**, 255–285. [Find this article online](#)
- Stern M. E., 1967: Lateral mixing of water masses. *Deep-Sea Res.*, **14**, 747–753. [Find this article online](#)
- Toole J. M., and D. T. Georgi, 1981: On the dynamics of double-diffusively driven intrusions. *Progress in Oceanography*, Vol. 10, Pergamon, 123–145.
- Turner J. S., 1968: The influence of molecular diffusivity on turbulent entrainment across a density interface. *J. Fluid Mech.*, **33**, 639–656. [Find this article online](#)
- Walsh D., and B. Ruddick, 1995: Double-diffusive interleaving: The influence of nonconstant diffusivities. *J. Phys. Oceanogr.*, **25**, 348–358. [Find this article online](#)
- Walsh D., 1998: Nonlinear equilibration of thermohaline intrusions. *J. Phys. Oceanogr.*, **28**, 1043–1070. [Find this article online](#)
- Zhang J., R. W. Schmitt, and R. X. Huang, 1998: Sensitivity of the GFDL Modular Ocean Model to parameterization of double-diffusive processes. *J. Phys. Oceanogr.*, **28**, 589–605. [Find this article online](#)

---

## Tables

TABLE 1. Representative observed water properties in the UPDW.\*

Property	Value
$T$	$-0.2\text{ }^{\circ}\text{C}$
$S$	34.90 psu
$\overline{T}_z$	$6.7 \times 10^{-7}\text{ }^{\circ}\text{C m}^{-1}$
$\overline{S}_z$	$6.4 \times 10^{-8}\text{ psu m}^{-1}$
$\overline{T}_z$	$1.0 \times 10^{-3}\text{ }^{\circ}\text{C m}^{-1}$
$\overline{S}_z$	$-6.4 \times 10^{-5}\text{ psu m}^{-1}$
$\alpha$	$7.7 \times 10^{-5}\text{ }^{\circ}\text{C}^{-1}$
$\beta$	$8.0 \times 10^{-4}\text{ psu}^{-1}$
$N_0$	$1.1 \times 10^{-3}\text{ s}^{-1}$
$\alpha\overline{T}_z/\beta\overline{S}_z$	1.0
$\alpha\overline{T}_z/\beta\overline{S}_z = R_T$	-1.5
$\overline{S}_z/\overline{S}_z = \Gamma_S$	-0.001

\* Sources: Anderson et al. (1994; Figs. 8–9) and Rudels et al. (1999; Figs. 2, 13–14).

[Click on thumbnail for full-sized image.](#)

TABLE 2. Sensitivity of intrusion height  $\lambda$ , slope  $s$ , and growth period  $r^{-1}$  to turbulent Prandtl number  $Pr$ , for  $K_T = 0.01\text{ cm}^2\text{ s}^{-1}$ ,  $K_S/K_T = 0.6$ , and  $\mu = 0$

$Pr$	$\lambda$ (m)	$s$	$r^{-1}$ (yr)
1	42	$4.6 \times 10^{-3}$	1.5
2	46	$4.4 \times 10^{-3}$	1.7
5	55	$4.1 \times 10^{-3}$	2.2

[Click on thumbnail for full-sized image.](#)

TABLE 3. *Oden* 91 stations used in determining along-intrusion density ratios  $R_T$

Station no.	Lat ( $^{\circ}\text{N}$ )	Long ( $^{\circ}\text{E}$ )
16	87 36.2	69 44.7
17	88 00.3	85 03.3
18	88 10.9	99 07.7
30	88 59.3	8 56.3
31	88 16.6	9 20.4
32	87 29.7	11 44.7

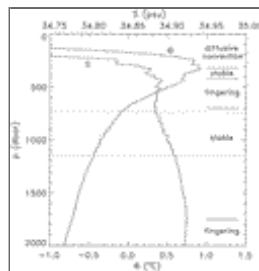
[Click on thumbnail for full-sized image.](#)

TABLE 4. Specification of effective diffusivities  $K_S$  and  $K_T$ , and effective viscosity  $A$  in numerical simulations

	Salt fingering $\rho_s < 0, 1 < R_T < \infty$	Diffusive convection $\rho_s < 0, 0 < R_T < 1$	Stable $\rho_s < 0, R_T < 0$	Convection $\rho_s \geq 0$
$R_T$	$\gamma \rho_s / \rho_s + \beta$	$\beta / \rho_s + \beta$	$\beta$	$\beta$
$K_T$	$K_T + K_T$	$\frac{1}{2} \rho_s A^2 + K_T$	$K_T$	$K_T$
$A$	$\text{Pr}(A) - \alpha_1 + \nu$	$\text{Pr}(A) - \alpha_1 + \nu$	$\text{Pr}(A) - \alpha_1 + \nu$	$\text{Pr}(A)$

[Click on thumbnail for full-sized image.](#)

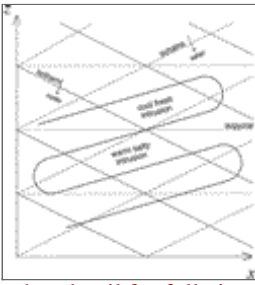
## Figures



[Click on thumbnail for full-sized image.](#)

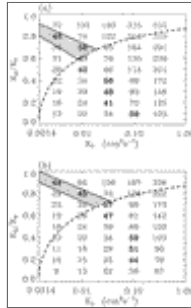
FIG. 1. Potential temperature and salinity sampled at 2-db intervals at *Oden* 91 station 17 ( $88^{\circ}00.3'\text{ N}$ ,  $85^{\circ}03.3'\text{ E}$ ) in Amundsen Basin, after [Anderson et al. \(1994\)](#). Approximate depth ranges having background gradients in the diffusive convective, salt fingering, and double-diffusively stable regimes are indicated, based on a subjective removal of the effects of intrusions from the  $\Theta$  and  $S$  profiles. Dotted lines bracket strong intrusive features in the stable Upper Polar Deep Water. (Here and elsewhere, observed salinity profiles have been smoothed using a two-point boxcar filter)





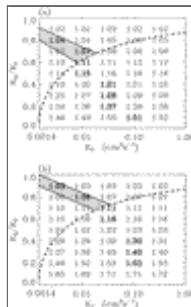
Click on thumbnail for full-sized image.

FIG. 2. Orientation of diffusively driven intrusions under double-diffusively stable conditions. Growing intrusions cross isopycnals more shallowly than the isohalines. If weak turbulence mixes  $T$  more effectively than  $S$ , rising intrusions can shed their negatively buoyant cold anomalies and grow



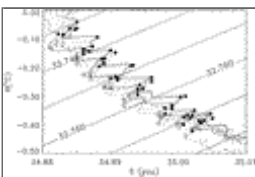
Click on thumbnail for full-sized image.

FIG. 3. Heights in meters of fastest-growing intrusions as functions of  $K_T$  and  $K_S/K_T$ , for  $Pr = 2$  and conditions in [Table 1](#) . Heights within the observed range 40–60 m are in bold face: (a)  $\mu = 0$  (constant  $K_T, K_S$ ), and (b)  $\mu = -1$  ( $K_T, K_S \propto N^{-1}$ ). The dashed curves indicate approximate lower bounds to  $K_S/K_T$  based on [Merryfield et al. \(1998\)](#), and the hatched regions admitted values for  $K_T$  and  $K_S/K_T$



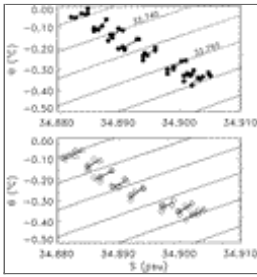
Click on thumbnail for full-sized image.

FIG. 4. Along-intrusion density ratios  $R_T$  of of fastest-growing intrusions as functions of  $K_T$  and  $K_S/K_T$ , for  $Pr = 2$  and conditions in [Table 1](#) : (a)  $\mu = 0$  (constant  $K_T, K_S$ ), and (b)  $\mu = -1$  ( $K_T, K_S \propto N^{-1}$ ). Values for which intrusion heights in [Fig. 3](#) are within the observed range 40–60 m are in bold face, and dashed curves indicate approximate lower bounds to  $K_S/K_T$  based on [Merryfield et al. \(1998\)](#). The hatched regions indicate  $K_T$  and  $K_S/K_T$  for which both constraints are met, as in [Fig. 3](#)



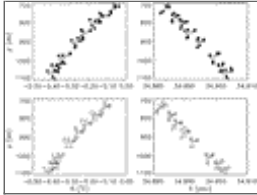
Click on thumbnail for full-sized image.

FIG. 5. Potential temperature–salinity profiles for intrusions in the UPDW, with  $\sigma_1$  contours superposed. Solid circles denote salinity maxima for individual intrusions, and open circles salinity minima. Data is from six *Oden 91* stations in the Amundsen Basin: station 16, thick solid; 17, thick dotted; 18, thick dashed; 30, thin dashed; 31, thin dotted; 32, thin solid



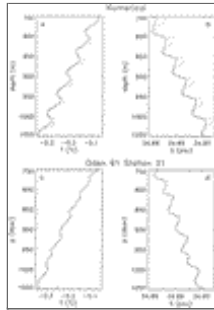
Click on thumbnail for full-sized image.

FIG. 6. Linear fits to intrusion salinity maxima (top) and minima (bottom) shown in Fig. 5. Intrusions rise across  $\sigma_1$  contours as they become warmer and saltier



Click on thumbnail for full-sized image.

FIG. 7. Pressures in db for intrusion salinity maxima (top) and minima (bottom) of Fig. 5, plotted against  $\Theta$  (left panels) and  $S$  (right). Intrusions tend to rise across isobars as they become warmer and saltier



Click on thumbnail for full-sized image.

FIG. 8. (a)–(b) Numerical solution of Eqs. (12)–(17) for  $K_T^0 = 0.01 \text{ cm}^2 \text{ s}^{-1}$ ,  $K_S^0/K_T^0 = 0.65$ , and  $\mu = 0$ . Solid curves denote an intermediate stage of growth, and dashed curves the nearly equilibrated intrusions. (c)–(d)  $T$  and  $S$  profiles observed at Oden 91 station 31 ( $88^\circ 16' \text{ N}$ ,  $9^\circ 20' \text{ E}$ )

Corresponding author address: William Merryfield, Canadian Centre for Climate Modelling and Analysis, Meteorological Service of Canada, University of Victoria, P.O. Box 1700, Victoria, BC V8W 2Y2, Canada. E-mail: [Bill.Merryfield@ec.gc.ca](mailto:Bill.Merryfield@ec.gc.ca)

<sup>1</sup> Coefficients  $K_T$ ,  $K_S$ , and  $A$  are defined to include molecular contributions  $\kappa_T$ ,  $\kappa_S$ , and  $\nu = 1.0 \times 10^{-2} \text{ cm}^2 \text{ s}^{-1}$ .

top ▲



